# Tissue engineering ECM-enriched controllable vascularized human microtissue for hair regenerative medicine using a biomimetic developmental approach

Peng Chen [1], Yong Miao [1], Feifei Zhang [1], Zhexiang Fan, Junfei Huang, Xiaoyan Mao, Jian Chen, Zhiqi Hu *, Jin Wang *

*Department of Plastic and Aesthetic Surgery, Nanfang Hospital, Southern Medical University, Guangzhou 510515, China*

## HIGHLIGHTS

- Layer-by-layer (LbL) self-assembly to construct nanoscale biomimetic ECM.
- Ca$^{2+}$ as a cross-linking agent to make size controllable dermal papilla (DP) spheroids.
- Tissue engineering controllable human microtissue rich in ECM and vessels.
- Vascularization prevents hypoxia-induced necrosis and functions in connection with host vessels.
- Biomimetic ECM and vascularization triple hair induction efficiency.

## GRAPHICAL ABSTRACT
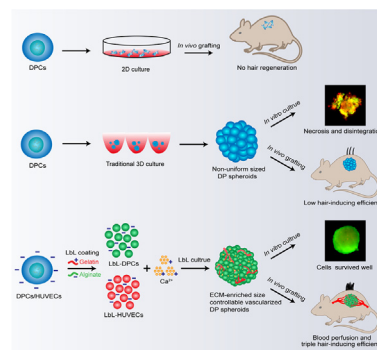
## ABSTRACT

*Introduction:* Regenerative medicine is a promising approach for hair loss; however, its primary challenge is the inductivity of human dermal papilla cells (DPCs), which rapidly lose hair growth-inducing properties in 2D culture. Despite extensive research efforts to construct DPCs, current 3D microenvironments fabricated to restore hair inductivity remain insufficient.
*Objectives:* Here, we aimed to fabricate ECM-enriched controllable vascularized dermal papilla (DP) spheroids that highly mimic *in vivo* DPCs microenvironments to restore their hair inductivity.
*Methods:* We employed layer-by-layer (LbL) self-assembly using gelatin and alginate to construct nanoscale biomimetic ECM for DPCs, with Ca$^{2+}$ as a cross-linking agent to create controllable DP spheroids. DPCs were also co-cultured with human umbilical vein endothelial cells to construct vascularized DP spheroids. Immunofluorescence staining and angiography was used to detect angiogenesis *in vitro* and *in vivo*. RNA sequencing and *in vivo* implantation were employed to investigate DPCs signature.
*Results:* LbL technology enabled DPCs to aggregate into controllable DP spheroids of size and cell numbers similar to those of primary DP. Vascularization prevented hypoxia-induced necrosis and functioned in association with host vessels post-transplantation. Compared with traditional 3D culture, nanoscale ECM and vascularization were found to restore the transcriptional signature of DPCs and triple hair induction efficiency following engraftment.

---

*Conclusion:* Our novel biomimetic developmental tissue engineering strategy is a crucial step toward the recovery of human DPC hair inductivity, which would enable the rapid clinical application of large-scale hair regeneration platforms.

## Introduction

Tissue engineering has become a promising approach for repairing damaged organs, and a useful platform for drug testing and disease modeling [1–3]. As a kind of mini organ with periodic regeneration and abundant sources, the hair follicle (HF) offers an attractive model for regenerative medicine. In addition, the number of patients experiencing hair loss is gradually increasing with an increasingly younger population being affected, whereas current treatments for hair loss, including medication and autologous hair transplantation, are limited and challenged by the inability to regenerate *de novo* HFs [4–5]. Therefore, tissue engineering of new HFs presents a promising solution for treating hair loss [6].

HFs are an ectodermal organ, composed of mesenchyme and epithelium. Dermal papillary cells (DPCs), as a highly specialized mesenchymal cells, are essential for HF cycling and morphogenesis [7]. In vivo, DPCs are surrounded by the extracellular matrix (ECM) and blood vessels, clustered into a specialized three-dimensional (3D), spherical structured dermal papilla (DP). Meanwhile, the application of HF tissue engineering as a viable therapeutic strategy requires a large number of DPCs with hair inductivity, a property that is rapidly lost in 2D culture due to the absence of the 3D microenvironment [8–9]. In an attempt to restore the inductive characteristics of DPCs, various approaches have been adopted to construct DP spheroids, such as hanging drop culture [10], low-adhesion biomaterial surfaces [11–12], and hydrogel culture [13–15]. Together these methods provide limited nutritional support, ECM imitation, or mass production of spheroids. Indeed, none have successfully mimicked the DPC niche *in vivo*, which comprises precisely-sized spheroids, rich in ECM and blood vessels. Furthermore, previous studies reported that approximately 12 hairs/50 spheroids could be generated by transplanting human DP aggregates into nude mice [12,16]. Therefore, enhancing the HF inductivity of cultured human DPCs remains a priority for advancing the bioengineering field of clinical HF regeneration.

Here, we attempted to develop an *in vitro* culture system with precisely-sized spheroids, rich in ECM and blood vessels that can mimic the *in vivo* niche to restore human DPCs biological function. To facilitate the construction of precisely controllable spheroids and the specific ECM for DPCs, we employed the layer-by-layer (LbL) self-assembly technology, which provides a potential approach for cell surface engineering. This entails a fabrication technique for coating cells with thin-film by depositing multi-coating layers of oppositely charged material-polycations and polyanions [17–18]. Due to its unique advantages, LbL technology has been widely used in various biomedical applications, including targeted gene therapy [19–20], biosensors [21–22], controlled drug delivery [23–24], and tissue engineering [25–27]. Polysaccharides and protein-based multilayer film are specifically considered to be a promising method for engineering nano-biomimetic ECM [28]. Due to their biocompatibility and biodegradability, alginate, a natural polysaccharide derived from algae, and the protein derivative, gelatin, have been broadly applied in ECM engineering [29–32]. Further, as the cell surface is coated with polyelectrolytes, single cells can aggregate into cell spheroids under ionic cross-linking [33]. As such, we chose gelatin and alginate to coat DPCs for ECM engineering in our study. $Ca^{2+}$ as a cross-linking agent was used to make a controllable DP spheroid to better imitate natural intercellular DPCs structures.

Currently, the primary limitation in tissue engineering is the lack of adequate vessel systems, that is vascularization [34]. Hence, due to insufficient nutrition and oxygen supply, cells in the 3D culture system typically undergo progressive necrosis in the center of spheroids, thereby reducing cell characteristics and functions [35]. Although studies have confirmed the presence of hypoxia-induced cell necrosis within DP spheroids [16], there is insufficient information to provide a reasonable solution to this critical issue. Moreover, recently, studies have focused on the use of spheroids as vascularized microtissue in tissue engineering [36–37], as vascularization is not only a potential strategy for rapidly establishing sufficient blood perfusion after implantation, but it also promotes the functionality of co-cultured cells [38], including vascularized pancreatic beta-cell spheroids, which promote insulin secretion, and neurovascularization, which enhances the function of engineered neural implants [39]. However, the current research has not yet constructed vascularized DP spheroids. whether vascularization can promote DPC function, connect with host vessels after transplantation, and improve HF induction efficiency, requires further investigation. Here, we constructed vascularized DP spheroids to elucidate these questions.

In this study, we developed an innovative biomimetic approach to efficiently generate HF by reconstructing the physiological 3D conformation of DPCs in an attempt to mimic the *in vivo* DP niche. We employed the LbL technique to construct nanoscale ECM for DPCs and $Ca^{2+}$ as a cross-linking agent to generate precisely controllable 3D DP spheroids. Furthermore, DPCs were co-cultured with human umbilical vein endothelial cells (HUVECs) to construct vascularized DP spheroids. We then explored how HUVECs influence the function of DPCs. Our approach permits the precise formation of controllable vascularized DP spheroids in a physiologically relevant ECM, as well as initiation of DPC – HUVEC interactions, which highly mimic the *in vivo* DP niche to restore the transcriptional signature of intact DPCs and promote HF formation. Therefore, this method presents a novel bioengineering strategy to achieve a reproducible, highly regenerative HF for clinical application. Moreover, this method allows for the study of regulatory mechanisms between endothelial cells and DPCs.

## Materials and methods

### Ethics statement

All mouse care and handling were carried out with the approval of the Institutional Animal Care and Use Committee of Southern Medical University, (Approval no. L2017048). Under the approval of the Medical Ethical Committee of Southern Medical University, human HFs were obtained from hair transplantation surgeries via follicular unit extraction (FUE). Informed consent was obtained from all participants.

### Preparation of human DPCs, HUVECs and newborn mice epidermal cells (EPCs)

The human HFs were microscopically separated to obtain the DP region and subsequently digested at 37 °C for 1 h with 0.2 % collagenase (Sigma-Aldrich, St. Louis, MO, USA) with shaking every 20 min. After centrifugation and washing, primary DP were trans-

ferred and cultured with 10 % fetal bovine serum (FBS; Gibco). Cells at passage four (*P4*) were obtained for subsequent experiments. HUVECs were purchased from Sciencell.

For isolation of EPCs, the skin of newborn C57BL/6J mice was removed, washed with PBS, and digested at 37 °C for 1 h with 0.1 % dispase (ThermoFisher Scientific, Waltham, MA, USA). Forceps were then used to separate the skin sample into the epidermis and dermis, after which the epidermis was cut into pieces and digested with 0.05 % trypsin (Gibco) for 5–10 min. Digestion was stopped with 10 % FBS solution, and the sample was filtered with a 40 μm strainer. After centrifugation for 5 min at $300 \times g$ and washing by DPBS, EPCs were obtained.

### LbL coating of individual DPCs

A total of $2 \times 10^6$ DPCs were added into a 15 mL centrifuge tube. Subsequently, 0.1 % gelatin (1 mL; Invitrogen, Carlsbad, CA, USA) solution was added and gently shaken on ice for 10 min. The supernatant was then discarded after centrifugation for 5 min at $300 \times g$. Then, the cell precipitates were washed twice, 0.1 % alginate (1 mL; Sigma-Aldrich) solution was added as the second coating layer. The same steps were then followed to apply another layer of gelatin and alginate, resulting in four-layered LbL nano-coated DPCs.

### Establishment of LbL-DP spheroids (LbL-DP) and vascularized DP spheroids (vascular DP)

For the preparation of LbL-DP, LbL nano-coated DPCs were resuspended and added to a 96-well low-adhesive plate. To each well, 1 μL of 0.1 M CaCl₂ solution was added. For vascular DP, LbL-DPCs and LbL-HUVECs (prepared with the same procedure as for LbL-DPCs) were mixed at different cell ratio and added to a 96-well low-adhesive plate. To each well, 1 μL of 0.1 M CaCl₂ solution was added. Uncoated DPCs were added to a 96-well low-adhesive plate at $1 \times 10^4$ cells/well in 200 μL medium, and the spheroids with a diameter of approximately 200 μm were chosen as the control group (con-DP).

### Preparation of fluorescently labeled materials

Commercially available gelatin-FITC was purchased from Invitrogen. To prepare alginate-rhodamine B, rhodamine B (20 mg; Invitrogen), 1-hydroxy-2, 5-pyrrolidinedione (NHS; 35 mg; Biovision, Milpitas, CA, USA), and 1-ethyl-3-(3(dimethylamino) propyl) carbodiimide (EDC; 40 mg; ThermoFisher Scientific) were added to 2 mL of DPBS and incubated for 30 min. Then ethylenediamine was added and stirred for 12 h, followed by dialysis and lyophilization to obtain rhodamine B-ethylenediamine powder. Next, 4 mL of 0.1 % alginate was mixed with the rhodamine B-ethylenediamine powder, and stirred for 12 h at RT. The mixture was then dialyzed and lyophilized to acquire alginate-rhodamine B powder.

### Transmission electron microscopy (TEM)

Samples were fixed with 2.5 % glutaraldehyde (Macklin, Shanghai, China) at 4 °C for 4 h and subsequently dehydrated and dried. After slicing into ultrathin sections, the cells were stained with uranyl acetate and lead citrate. Samples were then photographed using a Tecnai-10 microscope (Philips, Amsterdam, Netherlands).

### Scanning electron microscopy (SEM)

Samples were fixed with 2.5 % glutaraldehyde (Macklin, Shanghai, China) at 4 °C for 4 h, and subsequently dehydrated with ethanol. The cells were then sprayed with gold and photographed using a JSM-6330F (JEOL, Tokyo, Japan).

### Zeta potential

The zeta potential of uncoated DPCs and DPCs coated with different layers of LbL was determined using the Zeta potential analyzer.

### Live and dead cell staining

On days 3, 7, and 14 of culture, all samples were stained at 37 °C for 20 min using a Live/Dead Viability Kit (Invitrogen, L3224). A motorized inverted microscope (IX73, Olympus, Tokyo, Japan) was then applied to obtain images.

### Immunofluorescence

The cultured DPCs and DP spheroids were fixed with 4 % paraformaldehyde. Then they were permeabilized in 01 % Triton X-100 (Beyotime, Wuhan, China) and blocked with 1 % BSA (Beyotime). The samples were then treated with primary antibodies against Ki67 (1:250, Abcam; Cambridge, MA, USA), alkaline phosphatase (ALP) (1:200, Abcam), β-catenin (1:100, Abcam), α-SMA (1:200, Abcam), and CD31 (1:50, Abcam) at 4 °C for 16 h. Samples were subsequently treated with Alexa Fluor488- (1:250, Abcam) or Alexa Fluor647-conjugated secondary antibodies for 70 min at RT. Images were characterized using a confocal laser scanning microscopy (CLSM) (LSM880, Cari Zeiss, Jena, Germany) or fluorescence microscope (IX71 FL, Olympus).

### Quantitative real-time polymerase chain reaction (qRT-PCR)

Total RNA was isolated from samples using TRIzol (Invitrogen). The SYBR PrimeScript RT-PCR kit was used to synthesize cDNA from 2 mg of RNA, according to the manufacturer's instructions. The SYBR PrimeScript RT-PCR kit was used on the Stratagene MX3005P QRT-PCR system (Agilent Technologies, Santa Clara, CA, USA) according to the manufacturer's procedures. The primer sequences are listed in Table S1.

### Western blotting

Cell lysates were electrophoresed on a 2 % sodium lauryl sulfate–polyacrylamide gel. After blocking with 3 % BSA, the membrane was then treated with the following primary antibodies: ALP (1:800, Abcam), β-catenin (1:800, Abcam), α-SMA (1:800, Abcam), HIF1α (1:800, Abcam), IL-1β (1:800, Abcam), IL-6 (1:800, Abcam), TNF-α (1:800, Abcam), and RIP3 (1:800, Abcam) for 12 h at 4 °C. Appropriate secondary antibodies were then added (1:1000, Abcam) and incubated at RT for 70 min. Blots were analyzed using Odyssey infrared fluorescence scanning imaging system (Li-COR Biosciences, Lincoln, NE, USA).

### In vivo vascularization detection

First, DPCs were labeled by DID using the Multicolor Cell-Labeling kit (5 μL DID for 100 mL solution; Invitrogen V22889) for 20 min. The DPCs were then washed with DPBS twice for subsequent experiments. The procedure of labeling HUVECs with DIL (Invitrogen) was the same as that described above. The fluorescently labeled DPCs and HUVECs were used to prepare vascular DPs (40 aggregates/site), which were combined with $1.44 \times 10^5$ newborn mice EPCs and transplanted subcutaneously into nude mice. After 3 weeks, 5 % FITC-labeled dextran (50 μL; molecular weight: 150,000 Da; Sigma-Aldrich) was injected into mice tail veins. Nude mice were sacrificed 30 min later, frozen sections (20 μm/section) were taken from the transplantation site and pho-
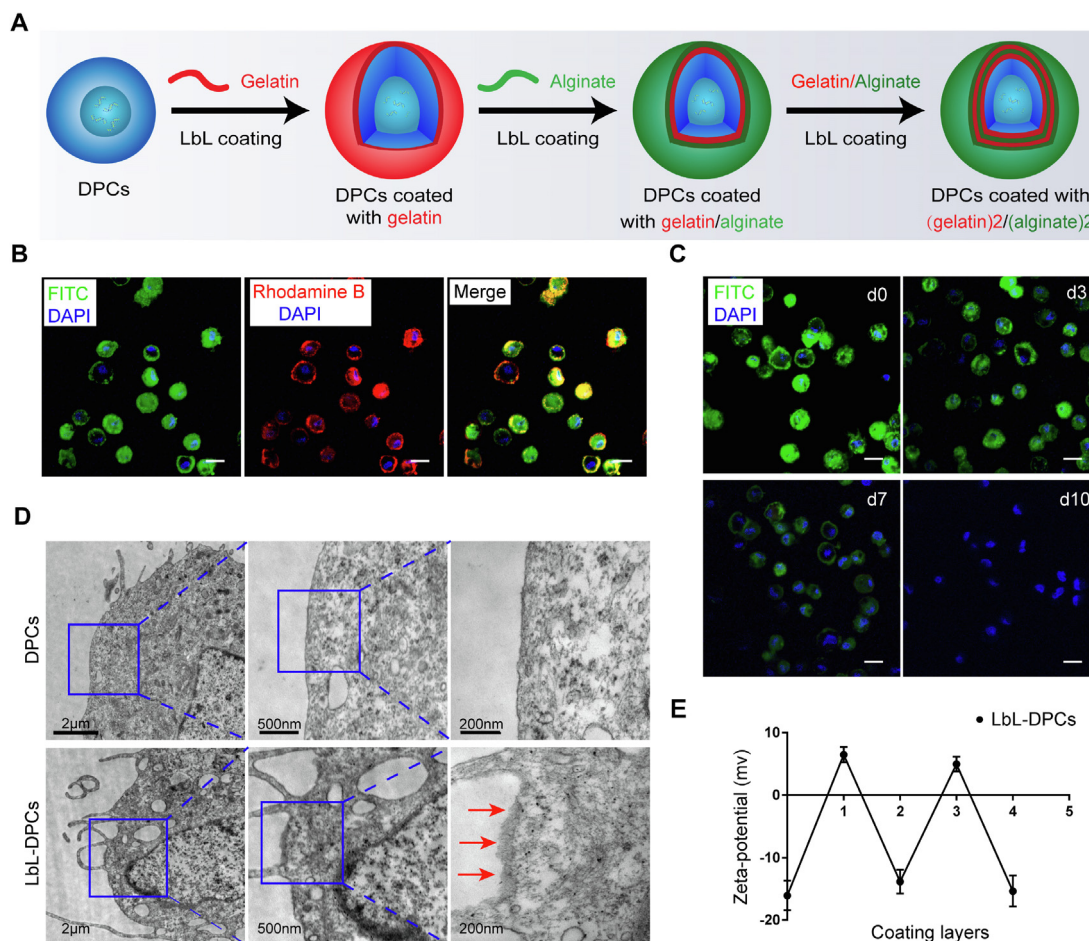
**Fig. 1.** Generation of LbL-DPCs by applying the LbL technique. **(A)** Schematic illustration of the fabrication of LbL-DPCs coated with gelatin (red) and alginate (green). **(B)** DPCs coated by gelatin-FITC (green) and alginate-rhodamine B (red). DAPI (blue); scale bars: 20 μm. **(C)** CLSM image displaying maintenance of the biomaterial following application of LbL coating. DAPI (blue); gelatin-FITC (green); scale bars: 20 μm. **(D)** TEM images comparing coated and uncoated DPCs. Red arrows indicate the biomaterials on the cell surface. **(E)** According to different coating layers, the corresponding zeta potential changes: (0) uncoated DPCs, (1) DPCs coated with gelatin, (2) DPCs coated with gelatin/alginate, (3) DPCs coated with (gelatin)2/alginate, (4) DPCs coated with (gelatin)2/(alginate)2.

tographed with a confocal microscope (LSM880, Cari Zeiss, Jena, Germany).

### In vivo fluorescence imaging

Gelatin-FITC coated DPCs was used to construct LbL-DP or vascular DP for *in vivo* fluorescence signal tracking. LbL-DP or vascular DP (40 aggregates/site) and $5 \times 10^5$ epidermal cells were injected subcutaneously into the dorsal sites of athymic nude mice. On 1, 3, and 7 days after injection, gelatin-FITC was detected using the In vivo FX Pro imaging system (Bruker, Madison, WI, USA).

### In vivo hair regeneration assay

The mice were anesthetized with sodium pentobarbital (1.3 mg/kg). DPCs/ DP spheroids with newborn mice EPCs in 50 μL DMEM subcutaneously injected in the dorsal side. Three weeks after *in vivo* transplantation, the injection sites were photographed with a stereomicroscope. The grafted areas were harvested, fixed, and embedded. Subsequently, samples were cut into sections (4 μm) and stained by hematoxylin and eosin (HE). Representative sections were then selected to be imaged and analyzed.

### RNA sequencing

TRIzol was used to isolate total RNA from each sample. Each sample was a mixture of cells from three different donors. Sequencing libraries were generated using NEBNext®UltraTM RNA Library Prep Kit for Illumina® (NEB, Ipswich, USA) according to the manufacturer's instructions. Briefly, mRNA was purified from total RNA using magnetic beads attached by poly-T oligo. The mRNA was fragmented into small pieces and then reverse transcribed into cDNA to produce the final cDNA library. Library preparations were sequenced on an Illumina Hiseq 2500 platform and paired-end reads were generated.

### Statistical analysis

All data analyses were conducted using GraphPad Prism software (GraphPad, version 7.0) or SPSS software (SPSS, version 18.0). One-way analysis of variance (ANOVA) was used to compare different groups. The data are presented as mean ± standard deviation (SD). Each experiment was performed in triplicate. In particular, *in vivo* HF regeneration studies were performed in triplicate using cells from three different donors (biological replicates). For the assessment of *in vivo* hair generation efficiency, n = 10 under each condition were assessed. $p < 0.05$ was considered significant.
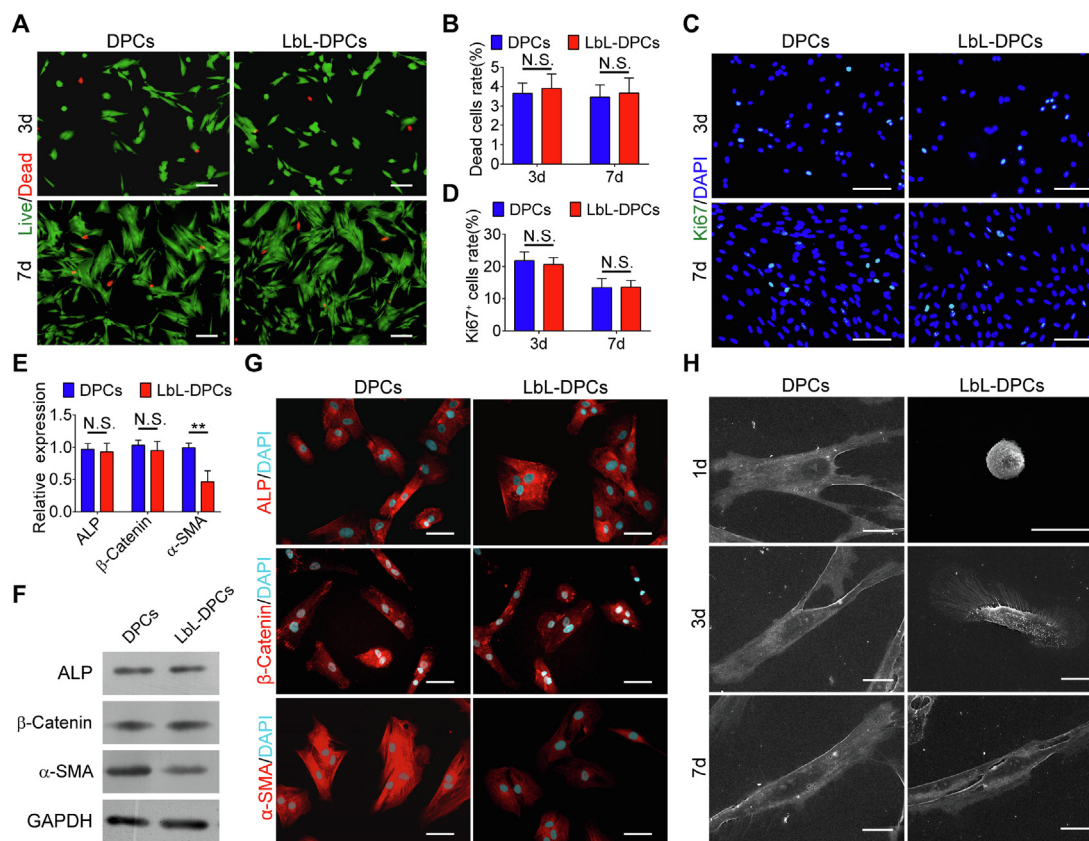
**Fig. 2.** LbL coating maintains DPC properties without damaging the cells. **(A-B)** On 3 d and 7 d of culture, DPC and LbL-DPC were Live and dead stained to assess cell viability. Live (red); dead (green); scale bars: 200 μm. **(C-D)** On 3 and 7 d of culture, DPC and LbL-DPC were stained with Ki67 immunofluorescence to detect cell proliferation. DAPI (blue); Ki67 (green); scale bars: 100 μm. **(E)** The qRT-PCR results showed *ALP*, *β-catenin*, and *α-SMA* mRNA expression. Relative fold expression of the DPCs is presented. **(F)** Western blot results showed ALP, β-catenin, and α-SMA protein expression. **(G)** Immunofluorescence staining 7 d post-coating to detect ALP, β-catenin, and α-SMA expression. DAPI (blue); ALP, β-Catenin, and α-SMA (red); Scale bars: 50 μm. **(H)** Morphological changes in DPCs and LbL-DPCs assessed by SEM. Scale bars: 20 μm. NS, not significant; **$p < 0.01$.

## Results

### Appropriately coated DPCs and their characteristics

ECM not only provides necessary signal transduction, but also provides physical support for cells and plays a vital role in cell function and growth [40–41]. Moreover, cytokine signal transduction in a cell–cell, cell-ECM or cell-niche manner, often occurs at the nanoscale [42]. To construct nanoscale ECM for DPCs, we initially extracted, cultured, and identified DPCs (**Figure S1**). We subsequently applied the LbL technique to coat the DPCs with gelatin/alginate (Fig. 1**A**). Gelatin-FITC and alginate-rhodamine B were applied uniformly on all cells via LbL nano-coating, and each respective coating exhibited green or red fluorescence (Fig. 1**B**). Further, the duration that the coating materials remained on the cell surface was observed using DPCs coated with (gelatin-FITC)-alginate-gelatin-alginate (Fig. 1**C**). The fluorescence intensity gradually decreased from 0 to 10 days, indicating that the coating material could be maintained for approximately 10 days.

In addition, TEM was conducted to demonstrate the presence of nano-matrix coating on LbL-DPCs compared to uncoated DPCs (Fig. 1**D**). Zeta potential analysis showed cell potential changes (5 mV, −40 mV) in response to different levels of biomaterial with the oppositely charged polyelectrolytes combining and depositing together (Fig. 1**E**). These results confirm that LbL coating has been successfully applied to DPCs.

### LbL coating enabled DPCs to maintain cell viability and properties

Next, we examined how the LbL coating affects DPCs. Live and dead staining was conducted at 3 d and 7 d post-coating (Fig. 2**A**). The results demonstrated that over a dynamic period, LbL coating had no significant effect on DPC viability ($p > 0.05$; Fig. 2**B**). Immunostaining for Ki-67 was also conducted at 3 d and 7 d post-coating, no significant differences were detected ($p > 0.05$; Fig. 2**C and D**). These results demonstrate that LbL coating with gelatin/alginate did not affect the DPCs viability or proliferation.

Additionally, qRT-PCR and western blot experiments demonstrated that the LbL coating maintained the signature genes/proteins expression including ALP and β-catenin, while inhibiting alpha-smooth muscle actin (α-SMA), a protein expressed in 2D cultured DPCs, but not in DP *in vivo* (Fig. 2**E and F**). The immunofluorescent staining results further validated these observations (Fig. 2**G**) demonstrating that LbL coating did not affect DPC properties.

To evaluate the morphological changes of cells, we applied SEM analysis of the uncoated and LbL-coated DPCs at different time points post-coating (Fig. 2**H**). The results demonstrated that the attachment of LbL-DPCs was slower than that of DPCs, and LbL-DPCs exhibited a more spheroid-like morphology, whereas the uncoated DPCs were broadly stretched. These results suggest that LbL-coated DPCs may morphologically exhibit more *in vivo*-like 3D structures.
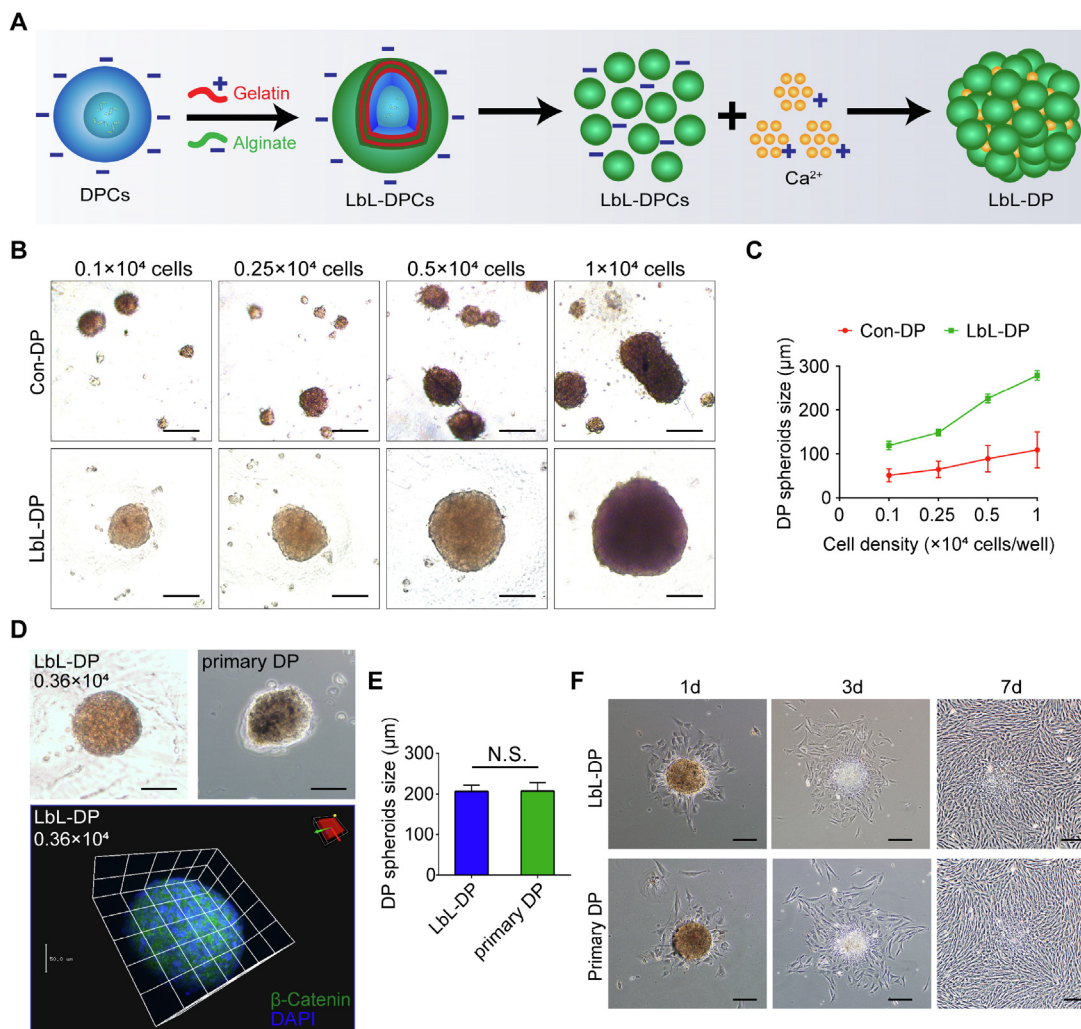
**Fig. 3.** Controllable DP spheroid formation. **(A)** Schematic diagram of the preparation of LbL-DP by coating DPCs with gelatin (red) and alginate (green), followed by $Ca^{2+}$ cross-linking. **(B)** Effects of different cell densities on DP spheroid formation 3 days after seeding. LbL-DPCs ($0.10$–$1 \times 10^4$ cells/well) aggregated into one spheroid in a regular manner, while the uncoated DPCs formed multiple spheroids (con-DP) of non-uniform size. Scale bars: 100 μm. **(C)** Effects of different cell densities on the size of DP spheroids. **(D)** Representative images showing the comparison between the LbL-DP ($0.36 \times 10^4$ cells/well) and the primary DP. 3D CLSM imaging revealed spherical structures of LbL-DP. DAPI (blue); β-catenin (green). **(E)** The sizes of LbL-DP showed no significant difference when compared to primary DP ($p > 0.05$). **(F)** The attachment, migration, and growth of LbL-DP was similar to that of freshly isolated primary DP. Scale bars: 100 μm; NS, not significant.

*Precisely controllable DP spheroids, rich in ECM are rapidly fabricated using LbL coating*

Previous research demonstrated that the 3D culture of human DPCs only partially restores their transcriptional signature. Meanwhile, the HF induction efficiency and hair number were generally influenced by the size/cell number of DP spheroid [12,43]. Therefore, to construct size/cell number-controllable DP spheroids is critical for human HF tissue engineering and future clinical applications.

Here, we applied gelatin as a polycation and alginate as a polyanion for nano-coating, and $Ca^{2+}$ as a cross-linking agent, to construct the ECM-rich DP spheroid with controllable size. Since the isoelectric point (IEP) at a neutral pH (7.4) differs, gelatin (IEP = 7–9) shows a positive charge, while alginate exhibits a negative charge. Gelatin was applied as the first layer on DPCs to provide cations, to which the anionic alginate was added as the second layer. Gelatin and alginate were sequentially deposited to the cell surface of the DPCs. When $CaCl_2$ solution was added to the LbL-DPCs, the alginate was ionically cross-linked by exposure to $Ca^{2+}$, and the LbL-DPCs aggregated to

form a single spheroid (LbL-DP; Fig. 3**A**) through culture on a low-adhesion plate for three days. The spheroid size increased with increasing cell density in the LbL-DP. However, the uncoated DPCs (as the control group) formed spheroids (con-DP) of non-uniform size after three days (Fig. 3**B and C**). This method could precisely control the size of DPC aggregates by adjusting the number of cells inoculated. In addition, by observing the morphology of the spheroids at different time points, we found that the LbL-DP aggregated most closely on day 3 (**Figure S2**). Thus, the optimum culture time was three days. Further, when the number of cells inoculated was 3600, we successfully constructed DP spheroids with a diameter of approximately 200 μm, similar to that of the primary DP isolated by our research group (Fig. 3**D and E**). Previous studies have confirmed that the cell number of human DP is 3–4000 with a diameter of 150–250 μm [10], which is consistent with the DP spheroids we constructed in terms of cell number and diameter.

To verify whether the LbL-DP remained viable and intact after transplantation *in vivo*, we carried out *in vitro* simulation experiments. LbL-DP were injected into the culture plate using a micropipette. The LbL-DP remained in a spherical shape and the cells
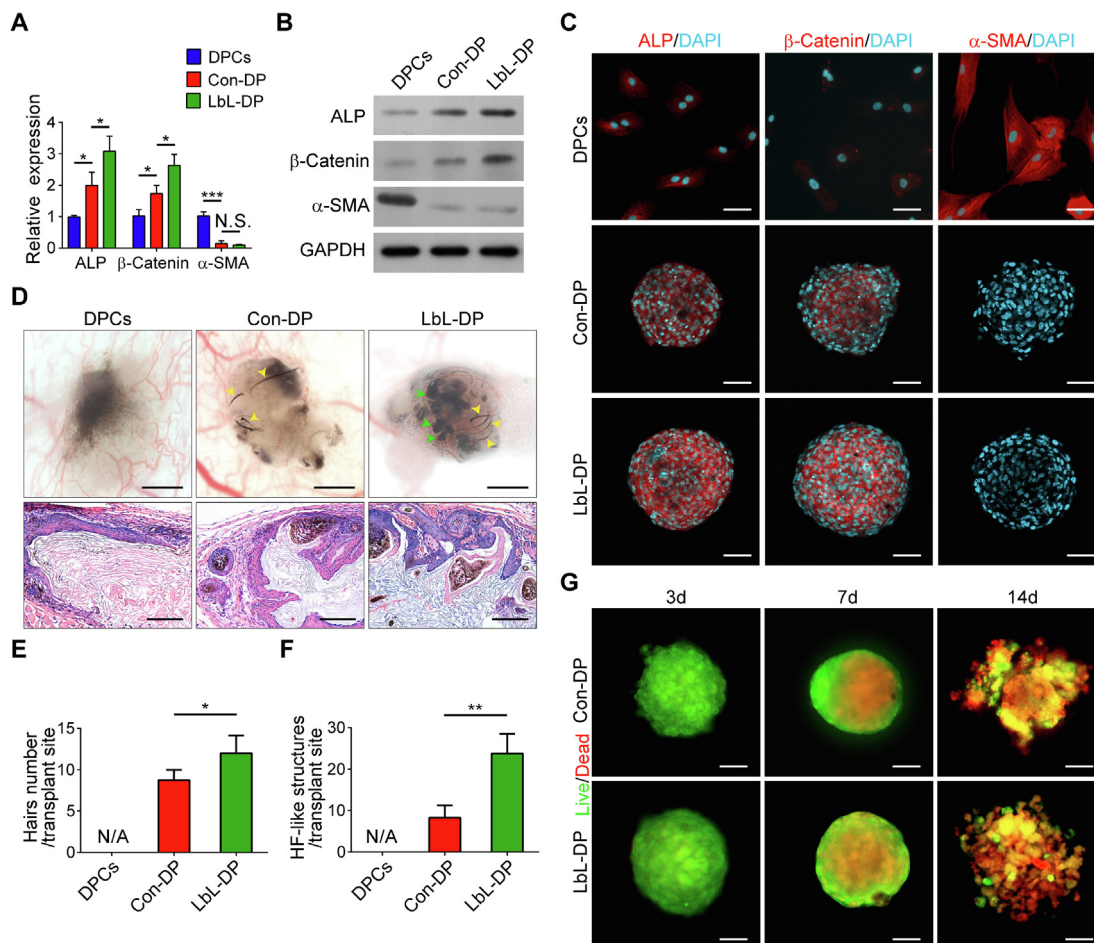
**Fig. 4.** LbL-DP signature gene and protein expression and hair inductivity. **(A)** qRT-PCR results showed *ALP*, *β-catenin*, and *α-SMA* mRNA expression, presented as relative fold expression of the 2D cultured DPCs. **(B)** Western blot results showed ALP, β-catenin, and α-SMA protein expression. **(C)** Immunofluorescence staining 7 d post-coating to detect the expression of ALP, β-catenin, and α-SMA in 2D cultured DPCs, con-DP, and LbL-DP. DAPI (blue); ALP, β-catenin, and α-SMA (red); Scale bars: 50 μm. **(D)** Stereoscopic images and HE staining of transplant sites three weeks post-injection. 2D cultured DPCs ($1.44 \times 10^5$ cells/site), con-DP (40 aggregates/site), and LbL-DP (40 aggregates/site) were co-transplanted with newborn mice EPCs. No hair was regenerated in 2D cultured DPCs, a small amount of *de novo* hair growth (yellow arrow heads) was induced by con-DP and LbL-DP, whereas many HF-like structures were generated in LbL-DP (green arrow heads). Scale bars: 100 μm (HE images) and 500 μm (stereoscopic images). **(E)** The LbL-DP population was most effective at inducing new hair growth. **(F)** LbL-DP also induces more HF-like structures than con-DP. **(G)** Live and dead staining of both con-DP and LbL-DP. Progressive cell death occurred in both groups. Live (green); Dead (red); Scale bars: 50 μm; NS, not significant; *$p < 0.05$; **$p < 0.01$; ***$p < 0.001$.

retained their ability to grow *in vitro* after passing through the micropipette tip (Fig. 3**F**). The results showed that the structural integrity and cell viability were preserved after LbL-DP injection.

### *LbL-DP partially restored the hair-inducing properties of human DPCs*

To characterize intrinsic properties of LbL-DP related to HF inductivity, we detected the major signature markers including ALP, β-catenin, and α-SMA. Both the con-DP and LbL-DP restored the expression of ALP and β-catenin, while suppressing that of α-SMA. Expression of ALP and β-catenin in LbL-DP was higher than that in con-DP (Fig. 4**A-C**). Even though these signature markers are an indicator of LbL-DP hair inductivity *in vitro*, the hair inductivity of LbL-DP needs further investigation *in vivo*. The interaction between epithelial and mesenchymal components stimulates hair follicle morphogenesis, and co-transplanting them can induce hair regeneration. For *in vivo* implantation, the cells were divided into three groups: *P*4-2D cultured DPCs ($1.44 \times 10^5$ cells/site), con-DP (40 ggregates/site) and LbL-DP (40 aggregates/site). Each group with $1.44 \times 10^5$ newborn mice EPCs were injected subcutaneously into the dorsal side. Surprisingly, after three weeks of implantation,

although the LbL-DP formed the most hair, as expected, and was superior to that of the con-DP and 2D cultured DPCs, the number of regenerated hair was as low as 29 % of the injected LbL-DP, with more producing HF-like structures, approximately 58 % (Fig. 4**D-F**). Our experimental results are consistent with previous studies showing very low hair-inducing efficiency of human DPCs, even in DP spheroids [12,16].

We suspected that the reason for the low hair induction efficiency of DP spheroids was the hypoxia-induced necrosis inside the spheroids. To verify this, we used live and dead staining to continuously observe the cell viability of cultured DP spheroids. We found that con-DP and LbL-DP survived well on the first three days of culture, with a small amount of cell death on the third day, with a large number of cell deaths at the spheroid center on the 7th day, and necrosis and disintegration of the entire spheroid on the 14th day (Fig. 4**G**). The results of immunofluorescence of Ki67 also showed that there were fewer proliferating cells in the con-DP and LbL-DP during the first three days, and almost no cell proliferation on the 7th and 14th days post-culture (**Figure S3**). Further, the gene expression of hypoxia-induced factor 1α (*HIF1α*) and necrosis markers [tumor necrosis factors-α (*TNF-α*); receptor-
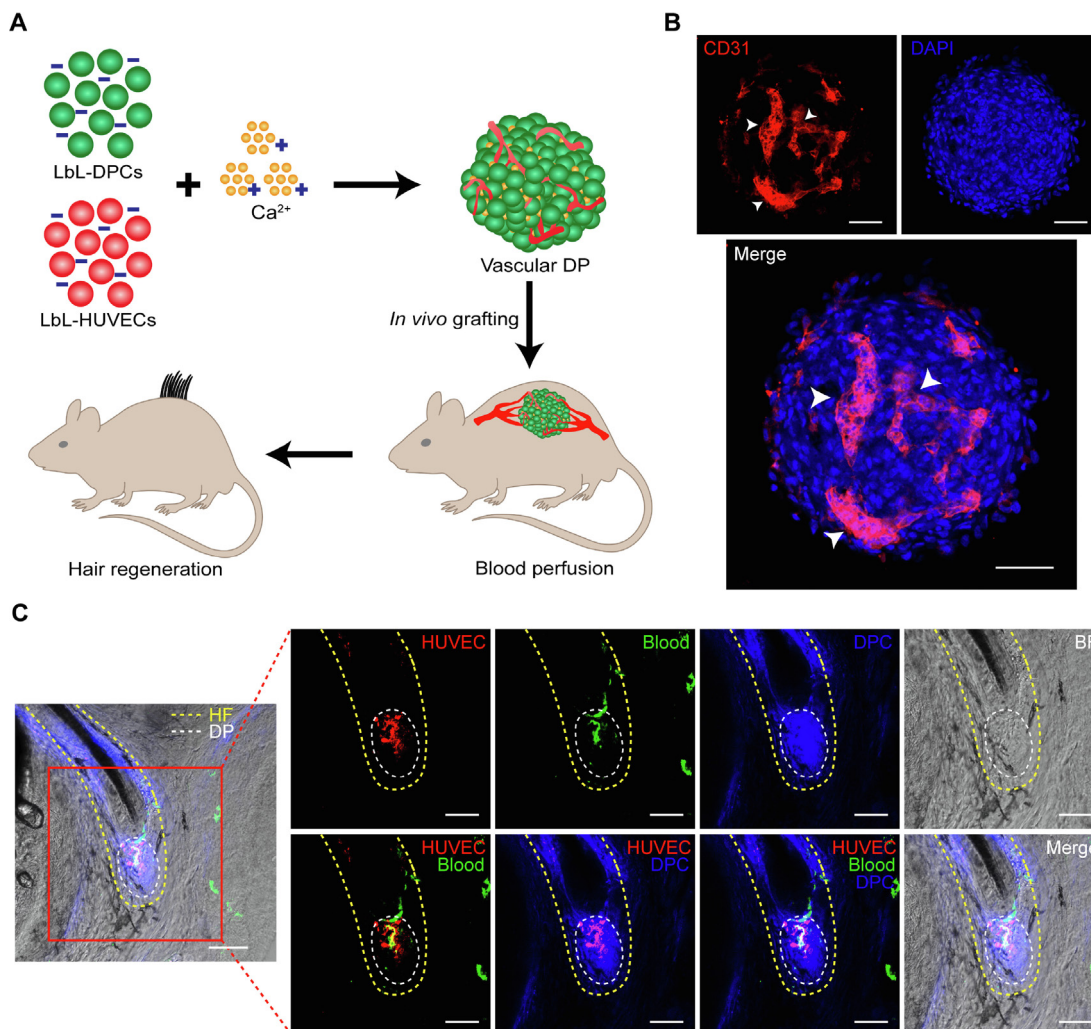
**Fig. 5.** LbL-DP spheroids vascularized *in vitro* and formed blood perfusion *in vivo*. (**A**) Schematic illustration the fabrication of vascular DP using LbL coating and the *in vivo* grafting to form blood perfusion and generate hair. (**B**) CD31 immunofluorescence staining of HUVECs showed clear vessel-like structures (arrow heads) inside the spheroids after three days of culture. DAPI (blue); CD31 (red); Scale bars: 50 μm. (**C**) CLSM images show new HF (yellow dotted line) generated after DP *in vivo* transplantation for three weeks. DPCs were labeled with DID in blue to form DP (white dotted line), which represents the DP spheroids constructed *in vitro*; HUVECs were labeled with DIL in red, which represents the vessels constructed *in vitro*; mouse blood was labeled with green fluorescence. The red-labeled HUVECs were only found in the blue-labeled DP and were perfused with green fluorescent-labeled mouse blood. Scale bars: 100 μm.

interacting kinase 3 (*RIP3*)] were upregulated in both con-DP and LbL-DP, and increased with culture time (**Figure S4**). This confirms that hypoxia leads to progressive necrosis of cells at the center of the spheroids.

*Generation of vascular DP*

In order to solve the problem of cell necrosis and low hair induction efficiency of the DP spheroids, vascularization seems to present a perfect solution, which not only improves hypoxia but also restores signal interaction between cells similar to the internal state to further improve cell function. To generate vascular DP, we mixed LbL-coated HUVECs with LbL-DPCs and inoculated with Ca²⁺ cross-linking (Fig. 5**A**). Thereafter, we co-cultured DPCs and HUVECs at different cell ratios (5:1, 3:1, 1:1, 1:3, 1:5), and finally chose the 3:1 DPCs to HUVEC ratio for the formation of vessel-like structures inside the spheroids (the total cell number was 3600; **Figure S5**). After three days of culture, we stained the endothelial cell marker CD31 with immunofluorescence to trace angiogenesis inside the spheroids. Whether in 2D or 3D immunofluorescence imaging, clear

vessel-like tubular structures were successfully constructed inside the spheroids (Fig. 5**B and Figure S6**).

Further, we used different fluorescent markers to label DPCs and HUVECs (DPCs as blue by DID and HUVECs as red by DIL) to verify whether the vessels constructed *in vitro* can be transplanted *in vivo* to exert blood perfusion functions. Next, the fluorescent-labeled DP spheroids combined with EPCs were transplanted *in vivo*. After three weeks 5 % FITC-labeled dextran (0.05 mL) was injected into nude mice via tail vein, and the blood was marked with green fluorescence, in order to visualize microvessels by contrast enhancement of the blood plasma. CLSM images show that vascular DP successfully promoted new hair growth, and the red-labeled HUVECs were found in the blue-labeled DP, and was perfused with green-labeled mouse blood (Fig. 5**C**). In addition, vascularization promoted the *in vivo* degradation of the coating materials due to increased blood perfusion (**Figure S7**). Our method not only successfully constructed the vascular DP *in vitro*, but also connected with the host blood vessels and formed blood perfusion after transplantation *in vivo*. This laid the foundation for HUVECs to regulate DPC function both *in vitro* and *in vivo*.
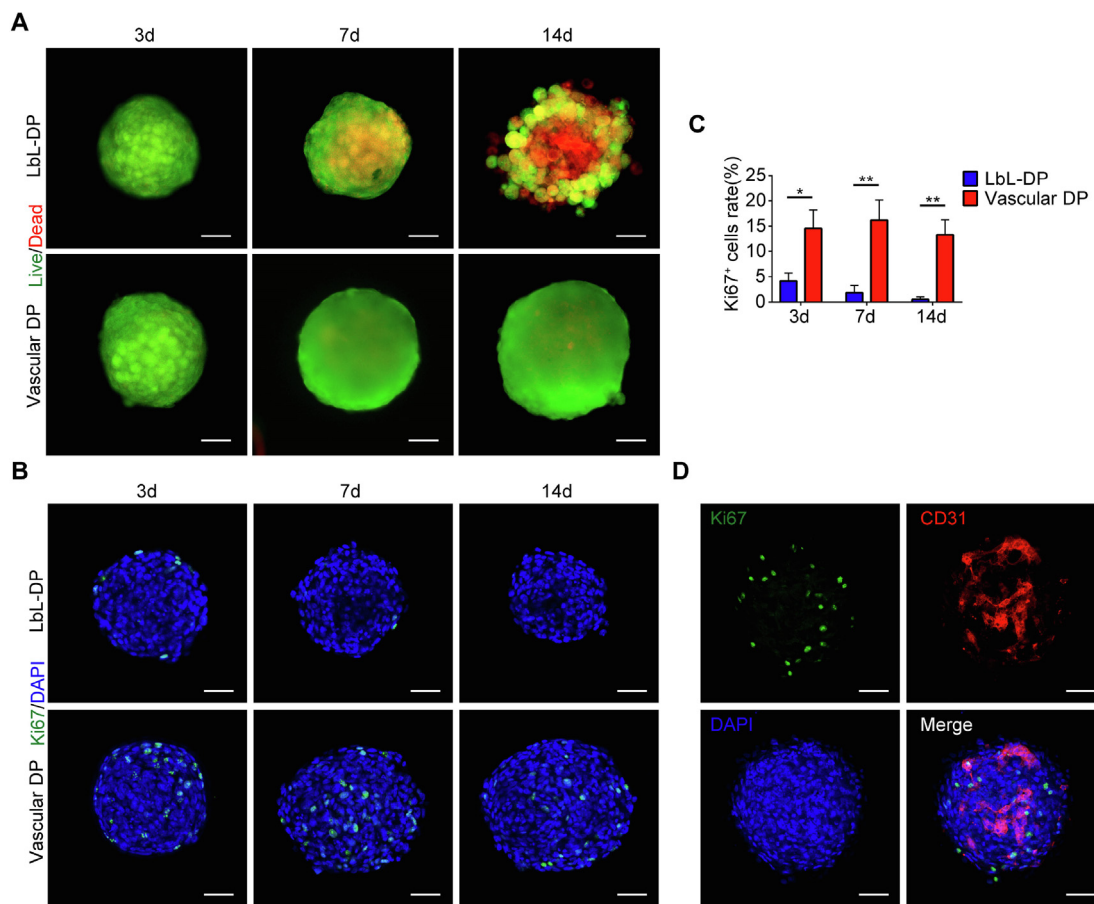
**Fig. 6.** Viability and proliferation of vascular DP. **(A)** Live and dead staining of both LbL-DP and vascular DP on day 3, 7, and 14 of culturing. Cells in the vascular DP survived well, whereas progressive cell death occurred in the LbL-DP. Live (green); Dead (red); Scale bars: 50 μm. **(B)** Cell proliferation detected by Ki67 immunofluorescence on day 3, 7, and 14 of culturing. DAPI (blue); Ki67 (green); Scale bars: 50 μm. **(C)** Ki67+ cells in vascular DP at different time points was significantly higher than that of LbL-DP. **(D)** Immunofluorescence co-staining of CD31 and Ki67 showed that the proliferating cells were DPCs, not CD31-labeled HUVECs. DAPI (blue); Ki67 (green); CD31 (red); *$p < 0.05$; **$p < 0.01$.

*Vascularization promotes cell survival and proliferation of DP spheroids*

Excitingly, we confirmed that vascular DP can significantly reduce cell death by live/dead staining. Even after the spheroids were cultured for 14 days *in vitro*, there was no obvious cell death in vascular DP, whereas LbL-DP exhibited necrosis and disintegration (Fig. 6A). Through morphological observation, we found that the vascular DP gradually contracted in the early stage of culture and gathered most closely on the third day, which was similar to LbL-DP. However, afterward, the vascular DP gradually increased spheroid size with cellular proliferation, but LbL-DP size did not change significantly ($p > 0.05$) until spheroid necrosis and disintegration on the 14th day (Figure S2). The Ki67 immunofluorescence further confirmed that the entire vascular DP maintained a high proportion of proliferating cells during *in vitro* culture, whereas the LbL-DP exhibited a small amount of cell proliferation at the edge of the spheroids in the first three days, with almost no proliferating cells after culture for seven days (Fig. 6B and C). We simultaneously applied immunofluorescence co-staining to confirm that the proliferating cells in the vascular DP were DPCs, excluding the false positive results, due to HUVEC proliferation (Fig. 6D).

*Vascular DP further promotes hair induction of human DPCs*

The primary issue in hair regeneration is the recovery of human DPC function. To characterize the intrinsic properties associated with HF inductivity in vascular DP, we examined the signature genes and proteins in vascular DP using qRT-PCR and western blot analysis. ALP and β-catenin expression in vascular DP were significantly higher than that of LbL-DP and DPCs, and vascular DP and LbL-DP suppressed the expression of α-SMA (Fig. 7A and B). The results of immunofluorescence staining further verified the above conclusions (Fig. 7C). These results confirm that vascularization can further promote hair inductivity of DPCs *in vitro*.

Further, to determine whether vascular DP was able to promote hair inductivity, *P*4-vascular DP (40 aggregates/site) mixed with EPCs ($1.44 \times 10^5$ cells/site) were implanted subcutaneously into nude mice. Three weeks after transplantation, considerable hair growth in the vascular DP was observed, but minor hair growth in LbL-DP, with numerous HF-like structures, which is consistent with the previous conclusion, hair growth was not induced in 2D cultured DPCs (Fig. 7D). Furthermore, we found that hair induction efficiency of the vascular DP was approximately 81 % of the injected DP spheroids, whereas that of the LbL-DP was only 29 % (Fig. 7E). The LbL-DP generated more HF-like structures (Fig. 7F). In vivo experiments showed that vascular DP could significantly enhance hair induction efficiency, as opposed to numerous HF-like structures in the LbL-DP.

*Improvement of HF induction by genetic reprogramming and anti-hypoxia*

To verify how vascularization promotes HF induction of DP spheroids, we performed RNA sequencing on 2D cultured DPCs, LbL-DP, and vascular DP three days post-culture at *P*4, as well as
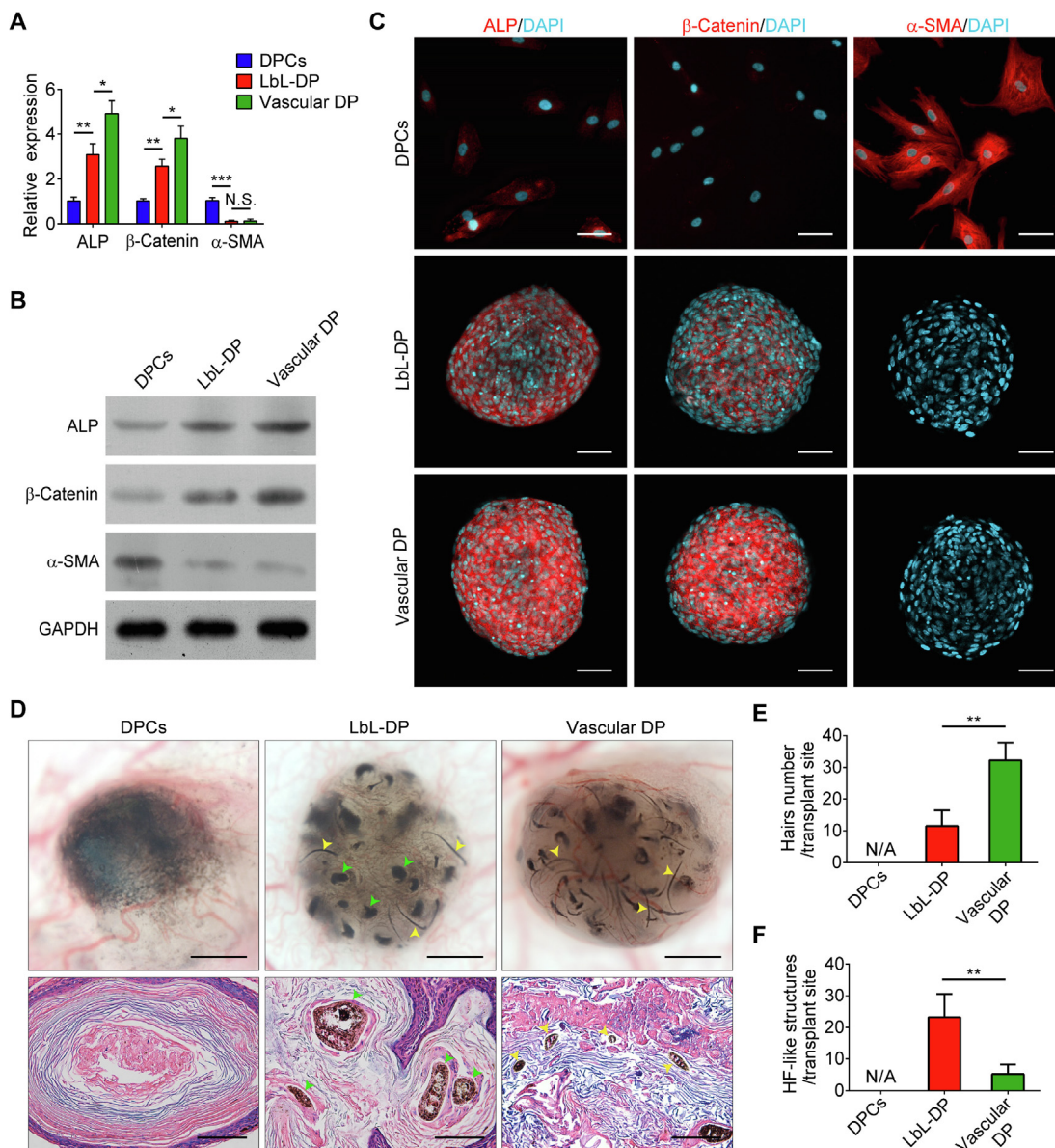
**Fig. 7.** Expression of signature genes and proteins in vascular DP and their hair inductivity. **(A)** qRT-PCR results showed *ALP, β-catenin*, and *α-SMA* mRNA expression. Data are presented as relative fold expression of the 2D cultured DPCs. **(B)** Western blot results showed ALP, β-catenin, and α-SMA protein expression. **(C)** Immunofluorescence staining of ALP, β-catenin, and α-SMA expression in 2D cultured DPCs, LbL-DP, and vascular DP. DAPI (blue); ALP, β-catenin, and α-SMA (red); Scale bars: 50 μm. **(D)** Stereoscopic images and HE staining of transplant sites after three weeks post-injection. DPCs ($1.44 \times 10^5$ cells/site), LbL-DP (40 aggregates/site) and vascular DP (40 aggregates/site) were co-transplanted with EPCs. In DPCs no hair regeneration was observed, while a large number of HF-like structures (green arrow heads) were induced by LbL-DP, and numerous *de novo* hairs were generated in vascular DP (yellow arrow heads). Scale bars: 100 μm (HE images) and 500 μm (stereoscopic images). **(E)** Vascular DP induced the maximum number of hairs. **(F)** LbL-DP induced more HF-like structures than vascular DP. NS, not significant; *$p < 0.05$; **$p < 0.01$. ***$p < 0.001$.

freshly isolated primary DP. The gene cluster heat map showed the difference in gene expression between four groups (Fig. 8A). Correlation analysis of gene expression levels showed that the correlation coefficient between vascular DP and primary DP was as high as 90 %, which was higher than 86 % in the LbL-DP and 83 % in the DPCs (Fig. 8B). This suggests that vascularization better restores DPC gene signature. In addition, by comparing differential gene expression of LbL-DP and vascular DP in the tumor necrosis factors (TNF) pathway (Fig. 8C), it was found that pro-inflammatory cytokines (e.g., IL-1β, IL-6, and TNF) were significantly down-regulated. Previous research confirmed that hypoxia–ischemia in tissues upregulates IL-1β, IL-6, and TNF leading to cell death [44]. Therefore, we hypothesize that vascularization can prevent DP spheroid necrosis caused by hypoxia. To test this hypothesis, we employed qRT-PCR and western blot analysis to

detect the expression of HIF1α, inflammatory factors (IL-1β, IL-6), and necrosis markers (TNF, RIP3). The results showed that vascularization significantly reduced their expression (Fig. 8D and E). These results confirmed that vascularization protects DP spheroids from necrosis caused by hypoxia.

## Discussion

Enhancing the HF inductivity of cultured human DPCs is one of the major challenges facing the bioengineering field for clinical HF regeneration [12]. Human DPCs transplanted as cell suspensions generate negligible amounts of hair, while engineering DP microtissues before *in vivo* transplantation was found to improve this process. Here, we have constructed a 3D co-culture system that
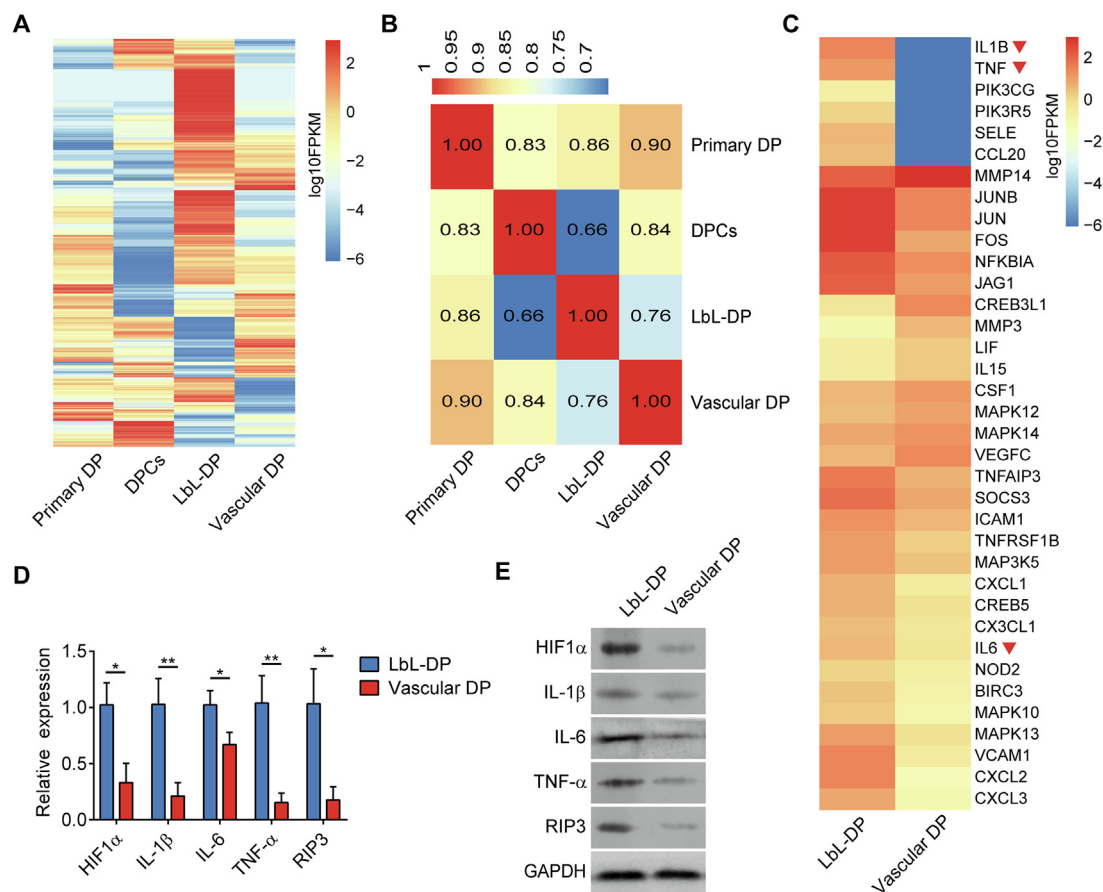
**Fig. 8.** Vascularization restores gene expression and prevents necrosis of spheroids caused by hypoxia. **(A)** Heatmap of quantified transcripts from RNAseq data generated from four groups, as primary DP, 2D cultured DPCs, LbL-DP, and vascular DP. **(B)** Sample correlation diagram showing the correlation between four samples (data shown as Pearson correlation coefficient). **(C)** Heatmap of TNF pathway-related genes with significant changes in LbL-DP and vascular DP (log2FC > 2, padj < 0.01). IL-1β, IL-6, and TNF are significantly down-regulated (red triangle). **(D)** The qRT-PCR analysis of *HIF1α*, *IL-1β*, *IL-6*, *TNF-α*, and *RIP3* mRNA expression. The data shown as relative fold expression of the LbL-DP. **(E)** Western blot results showed HIF1α, IL-1β, IL-6, TNF-α, and RIP3 protein expression. $*p < 0.05$; $**p < 0.01$.

can precisely control the size of the spheroids and is rich in ECM and vessels. This system can more reasonably and comprehensively simulate the DPC microenvironment, thereby significantly improving hair inductivity.

We applied biomaterial gelatin and alginate to coat individual DPCs using LbL technology to construct nanoscale ECM. Our results show that LbL coating does not cause damage to DPCs allowing them to maintain their cellular properties. In addition, the results from SEM demonstrated that LbL-coated DPCs exhibited *in vivo*-like 3D structures, suggesting that LbL coating provided mechanical support for DPCs to allow them to form a spherical state, similar to in the *in vivo* cell microenvironment. Although LbL coating maintained DPCs in a more spherical structure and down-regulated the expression of α-SMA in 2D culture, there was no difference in ALP and β-catenin expression. In the aggregated state, the LbL-DP significantly upregulated ALP and β-catenin expression compared to con-DP, which may be due to nanoscale ECM coated DPCs, which may be beneficial for both intercellular communication and bio-macromolecule transportation. The ECM is not only the basis for cell growth, but also a dynamic participant in tissue homeostasis and cellular crosstalk [45]. The application of native ECM polysaccharides and proteins as scaffolds provides a similar structure to natural ECM, mimicking the chemical and physical properties of cellular ECM *in vivo* [46]. Additionally, gelatin is a protein derivative and alginate is derived from algae [47], these two biomaterial were excellent biomaterials for nanoscale ECM engineering [48].

Further, when CaCl$_2$ solution was added to LbL-DPCs, alginate became ionically cross-linked by Ca$^{2+}$, enabling LbL-DPCs to aggregate into a single spheroid. Compared with traditional low-adhesion culture, our method can produce size/cell number-controllable DP spheroids, and a rich ECM to promote hair induction. The size/cell number of DP spheroids are critical for the bioengineering of HF regeneration. Previous studies have found that both human and rodent DPCs can induce HF regeneration when transplanted as spheroids. Small DP spheroids cannot induce hair regeneration, large DP spheroids will generate multiple hairs, and the diameter of the regenerated hair fibers does not change with the size of the transplanted DP spheroids [12,16,49]. These studies showed that the proper size of DP spheroids is vital for HF regeneration, by not only improving HF inductivity, but also regulating the hair number of single DP spheroids. Our method can produce controllable DP spheroids, with size and cell number similar to those of primary DP, and enables one DP spheroid to generate one hair shaft, which is beneficial for engineering clinically usable HFs.

Significant interspecies differences have not only been reported between human and rodent HFs regarding hair cycle, hormonal dependencies, and stem cell characteristics, but also in DPCs hair inductivity. One notable difference is that after transplantation *in vivo*, cultured rodent DPCs can self-aggregate, but not human DPCs [50]. Human DPCs could not regenerate new hair after several passages in 2D culture. Many studies have committed to solving this problem through 3D-spheroid culture, thereby partially recov-

ering the hair induction efficiency, but have not yet achieved efficient results [12,16]. This is consistent with our results. The hair induction efficiency in the con-DP was approximately 22 %, whereas LbL-DP was only approximately 29 %. The low induction efficiency of human DPCs has seriously hindered the progressive research on human HF regeneration.

In this study, we aimed to improve hair induction efficiency of human DPCs via the analysis of constructed DP spheroids, and found that, during the culture process, the cells suffer progressive hypoxia in the spheroid center, causing spheroid necrosis and disintegration. Therefore, to solve spheroid necrosis and construct a more biomimetic DP spheroid, we co-cultured DPCs with HUVECs to construct vascular DP. The results showed that vascular DP formed clear vessel-like tubular structures after three days of *in vitro* culture. Compared with the LbL-DP, vascularization did not only significantly reduce DP spheroid necrosis, but also promoted cell proliferation. With improved cellular proliferation, the size of the spheroid gradually increased, surviving for up to 14 days in *in vitro* culture, whereas LbL-DP exhibited necrosis and disintegration. More importantly, after *in vivo* transplantation, the pre-constructed vessels successfully connect with host vessels and form blood perfusion to perform their functions and increase the hair induction efficiency of LbL-DP from 29 % to 81 %. Our results showed that Con-DP and LbL-DP had less hair growth, LbL-DP induced more immature HF-like structures, and vascularization further promoted the maturation of HF-like structures to induce massive hair regeneration. This suggests that the biomimetic ECM constructed by LbL coating only partially restores the function of DPCs, whereas combined vascularization significantly enhances the hair inductivity of DPCs. This solves the most critical issue of engineering HFs, caused by insufficient hair induction efficiency of human DPCs. Using our method, we generally generated 18 million DPCs (*P*4) from 150 donor HFs, yielding enough cells to generate approximately 5000 new HFs, and presenting an efficient and feasible strategy ready to be integrated with hair restoration therapy.

Further, our results show that vascularization can not only prevent cell necrosis caused by hypoxia, but also restores the DPCs gene signature, with a similarity of 90 % to that of primary DP. Vascularization provides sufficient oxygen and nutrition to the spheroids, and also restores the signal interaction between endothelial cells and DPCs, thereby better promoting DPCs functions. Moreover, studies have confirmed that HF cycling and androgen alopecia were associated with vascularization levels of HFs. However, due to the complexity of the internal microenvironment and the lack of *in vitro* vascularization models, the specific mechanism between the endothelial cells and the DPCs is still unclear. Vascularized DP spheroids are not only a new strategy for tissue engineering of HFs, but also provide a research platform to study the interaction between endothelial cells and DPCs to elucidate potential mechanisms.

In this study, chimeric HFs consisting of human DPCs and mouse EPCs were verified. However, further investigations applying human-derived cells, preferably from patients experiencing hair loss, are needed. Previously, we have successfully applied LbL technology to construct a biomimetic microenvironment for human HF stem cells to expand them and reveal their plasticity [31,51]. We, therefore, expect to apply the LbL technology to combine human HF stem cells and vascularized DP spheroids to construct controllable biomimetic HF germ *in vitro,* and transplant *in vivo* to achieve human HF regeneration. In addition, growth factors/signal molecules loaded into LbL coating layers may further increase hair production efficiency. Using our approach, combining human HF stem cells and vascularized DP spheroids in co– cultures *in vitro* or co-transplantations *in vivo* will be a promising solution to achieving large-scale human HF regeneration.

## Conclusions

A key issue in hair regeneration medicine is the inductivity of human DPCs after expansion culture. The preparation of large-scale clinically available artificial HFs is also a critical concern. The present study demonstrated that LbL technology was able to construct nanoscale biomimetic ECMs for DPCs, and under the cross-linking of Ca2⁺, DPCs aggregated into a single spheroid with size and cell number similar to those of primary DP. After co-culture with HUVECs, the spheroid necrosis caused by hypoxia was solved, and DPC gene expression was restored. The size controllable DP spheroids, rich in ECM and endothelial cells, more realistically and comprehensively simulate the *in vivo* microenvironment of DPCs. Compared to conventional spheroid cultures, nanoscale ECM and vascularization restores the DPCs transcriptional signature, and *in vivo* transplantation of vascularized DP resulted in almost a threefold increase in the number of generated hair shafts. Our novel biomimetic developmental tissue engineering strategy is a crucial step in the recovery of human DPC hair inductivity and provides a new avenue for the fabrication of microtissues for hair regenerative therapy.

## Compliance with Ethics Requirements

All Institutional and National Guidelines for the care and use of animals (fisheries) were followed.

## Declaration of Competing Interest

The authors declare that they have no known competing financial interests or personal relationships that could have appeared to influence the work reported in this paper.

## Acknowledgments

## Appendix A. Supplementary material

Supplementary data to this article can be found online at https://doi.org/10.1016/j.jare.2021.09.010.

## References

[1] MacNeil S. Progress and opportunities for tissue-engineered skin. Nature 2007;445(7130):874–80.
[2] Atala A. Engineering organs. Curr Opin. Biotech. 2009;20(5):575–92.
[3] Redd MA, Zeinstra N, Qin W, Wei W, Martinson A, Wang Y, et al. Patterned human microvascular grafts enable rapid vascularization and increase perfusion in infarcted rat hearts. Nat Commun. 2019;10(1). doi: https://doi.org/10.1038/s41467-019-08388-7.
[4] Marshall BT, Ingraham CA, Wu X, Washenik K. Future horizons in hair restoration. Facial Plast Surg Cl. 2013;21(3):521–8.
[5] Chen Y, Huang J, Chen R, Yang L, Wang J, Liu B, et al. Sustained release of dermal papilla-derived extracellular vesicles from injectable microgel promotes hair growth. Theranostics. 2020;10(3):1454–78.
[6] Ohyama M, Veraitch O. Strategies to enhance epithelial-mesenchymal interactions for human hair follicle bioengineering. J Dermatol Sci. 2013;70(2):78–87.
[7] Abreu CM, Cerqueira MT, Pirraco RP, Gasperini L, Reis RL, Marques AP. Rescuing key native traits in cultured dermal papilla cells for human hair regeneration. J Adv Res. 2021;30:103–12.
[8] Ohyama M, Kobayashi T, Sasaki T, Shimizu A, Amagai M. Restoration of the intrinsic properties of human dermal papilla in vitro. J Cell Sci. 2012;125:4114–25.
[9] Abaci HE, Coffman A, Doucet Y, Chen J, Jacków J, Wang E, et al. Tissue engineering of human hair follicles using a biomimetic developmental

approach. Nat Commun. 2018;9(1). doi: https://doi.org/10.1038/s41467-018-07579-y.

[10] Lin B, Miao Y, Wang J, Fan Z, Du L, Su Y, et al. Surface Tension Guided Hanging-Drop: Producing Controllable 3D Spheroid of High-Passaged Human Dermal Papilla Cells and Forming Inductive Microtissues for Hair-Follicle Regeneration. Acs Appl Mater Inter. 2016;8(9):5906–16.

[11] Osada A, Iwabuchi T, Kishimoto J, Hamazaki TS, Okochi H. Long-term culture of mouse vibrissal dermal papilla cells and de novo hair follicle induction. Tissue Eng. 2007;13(5):975–82.

[12] Huang Y, Chan C, Lin W, Chiu H, Tsai R, Tsai T, et al. Scalable production of controllable dermal papilla spheroids on PVA surfaces and the effects of spheroid size on hair follicle regeneration. Biomaterials 2013;34:442–51.

[13] Driskell RR, Juneja VR, Connelly JT, Kretzschmar K, Tan DW, Watt FM. Clonal growth of dermal papilla cells in hydrogels reveals intrinsic differences between Sox2-positive and -negative cells in vitro and in vivo. In; 2012. p. 1084-93.

[14] Tan JJY, Common JE, Wu C, Ho PCL, Kang L. Keratinocytes maintain compartmentalization between dermal papilla and fibroblasts in 3D heterotypic tri-cultures. Cell Proliferat. 2019;52(5). doi: https://doi.org/10.1111/cpr.v52.510.1111/cpr.12668.

[15] Miao Y, Sun YB, Liu BC, Jiang JD, Hu ZQ. Controllable production of transplantable adult human high-passage dermal papilla spheroids using 3D matrigel culture. Tissue Eng Part A 2014;20:2329–38.

[16] Kageyama T, Yan L, Shimizu A, Maruo S, Fukuda J. Preparation of hair beads and hair follicle germs for regenerative medicine. Biomaterials 2019;212:55–63.

[17] Sousa MP, Arab-Tehrany E, Cleymand F, Mano JF. Surface Micro- and Nanoengineering: Applications of Layer-by-Layer Technology as a Versatile Tool to Control Cellular Behavior. Small 2019;15(30):e1901228.

[18] Guo S, Zhu X, Loh XJ. Controlling cell adhesion using layer-by-layer approaches for biomedical applications. Materials science & engineering. C, Materials for biological applications. 2017;70:1163–75.

[19] Elzoghby AO. Gelatin-based nanoparticles as drug and gene delivery systems: reviewing three decades of research. Journal of controlled release: official journal of the Controlled Release Society. 2013;172(3):1075–91.

[20] Gupta B, Ruttala HB, Poudel BK, Pathak S, Regmi S, Gautam M, et al. Polyamino Acid Layer-by-Layer (LbL) Constructed Silica-Supported Mesoporous Titania Nanocarriers for Stimuli-Responsive Delivery of microRNA 708 and Paclitaxel for Combined Chemotherapy. Acs Appl Mater Inter. 2018;10(29):24392–405.

[21] García-Alonso J, Fakhrullin RF, Paunov VN, Shen Z, Hardege JD, Pamme N, et al. Microscreening toxicity system based on living magnetic yeast and gradient chips. Anal Bioanal Chem. 2011;400(4):1009–13.

[22] Ketelsen B, Yesilmen M, Schlicke H, Noei H, Su C-H, Liao Y-C, et al. Fabrication of Strain Gauges via Contact Printing: A Simple Route to Healthcare Sensors Based on Cross-Linked Gold Nanoparticles. Acs Appl Mater Inter. 2018;10(43):37374–85.

[23] Lu J, Zhuang W, Li L, Zhang Bo, Yang Li, Liu D, et al. Micelle-Embedded Layer-by-Layer Coating with Catechol and Phenylboronic Acid for Tunable Drug Loading, Sustained Release, Mild Tissue Response, and Selective Cell Fate for Re-endothelialization. Acs Appl Mater Inter. 2019;11(10):10337–50.

[24] Zhao Q, Fan Y, Zhang Yu, Liu J, Li W, Weng Y. Copper-Based SURMOFs for Nitric Oxide Generation: Hemocompatibility, Vascular Cell Growth, and Tissue Response. Acs Appl Mater Inter. 2019;11(8):7872–83.

[25] Matsuzawa A, Matsusaki M, Akashi M. Effectiveness of nanometer-sized extracellular matrix layer-by-layer assembled films for a cell membrane coating protecting cells from physical stress. Langmuir : the ACS journal of surfaces and colloids. 2013;29(24):7362–8.

[26] Fukuda Y, Akagi T, Asaoka T, Eguchi H, Sasaki K, Iwagami Y, et al. Layer-by-layer cell coating technique using extracellular matrix facilitates rapid fabrication and function of pancreatic beta-cell spheroids. Biomaterials 2018;160:82–91.

[27] Lu Y, Li X, Zhou X, Wang Q, Shi X, Du Y, et al. Characterization and cytotoxicity study of nanofibrous mats incorporating rectorite and carbon nanotubes. Rsc Adv. 2014;4(63):33355. doi: https://doi.org/10.1039/C4RA03782K.

[28] Silva JM, Reis RL, Mano JF. Biomimetic Extracellular Environment Based on Natural Origin Polyelectrolyte Multilayers. Small 2016;12(32):4308–42.

[29] Wang J, Miao Y, Huang Y, Lin B, Liu X, Xiao S, et al. Bottom-up Nanoencapsulation from Single Cells to Tunable and Scalable Cellular Spheroids for Hair Follicle Regeneration. Adv Healthc Mater. 2018;7(3):1700447. doi: https://doi.org/10.1002/adhm.201700447.

[30] Rosellini E, Zhang YS, Migliori B, Barbani N, Lazzeri L, Shin SR, et al. Protein/polysaccharide-based scaffolds mimicking native extracellular matrix for cardiac tissue engineering applications. J Biomed Mater Res a. 2018;106(3):769–81.

[31] Chen P, Miao Y, Zhang F, Huang J, Chen Y, Fan Z, et al. Nanoscale microenvironment engineering based on layer-by-layer self-assembly to regulate hair follicle stem cell fate for regenerative medicine. Theranostics. 2020;10(25):11673–89.

[32] Li X, Feng J, Zhang R, Wang J, Su T, Tian Z, et al. Quaternized Chitosan/Alginate-Fe3O4 Magnetic Nanoparticles Enhance the Chemosensitization of Multidrug-Resistant Gastric Carcinoma by Regulating Cell Autophagy Activity in Mice. J Biomed Nanotechnol. 2016;12:948–61.

[33] Mao AS, Shin J-W, Utech S, Wang H, Uzun O, Li W, et al. Deterministic encapsulation of single cells in thin tunable microgels for niche modelling and therapeutic delivery. In 2017;16(2):236–43.

[34] Novosel EC, Kleinhans C, Kluger PJ. Vascularization is the key challenge in tissue engineering. Adv Drug Deliv Rev. 2011;63(4-5):300–11.

[35] Anada T, Fukuda J, Sai Y, Suzuki O. An oxygen-permeable spheroid culture system for the prevention of central hypoxiaand necrosis of spheroids. Biomaterials 2012;33(33):8430–41.

[36] Walser R, Metzger W, Görg A, Pohlemann T, Menger MD, Laschke MW. Generation of co-culture spheroids as vascularisation units for bone tissue engineering. Eur Cells Mater. 2013;26:222–33.

[37] Verseijden F, Sluijs S-V, Van Neck JW, Hofer SOP, Hovius SER, Van Osch GJVM. Comparing scaffold-free and fibrin-based adipose-derived stromal cell constructs for adipose tissue engineering: an in vitro and in vivo study. Cell Transplant. 2012;21(10):2283–97.

[38] Laschke MW, Menger MD. Prevascularization in tissue engineering: Current concepts and future directions. Biotechnol Adv. 2016;34(2):112–21.

[39] Shor E, Merdler U, Brosh I, Shoham S, Levenberg S. Induced neuro-vascular interactions robustly enhance functional attributes of engineered neural implants. Biomaterials 2018;180:1–11.

[40] Stevens MM, George JH. Exploring and engineering the cell surface interface. Science (New York, N.Y.). 2005;310:1135–8.

[41] Ghajar CM, Bissell MJ. Extracellular matrix control of mammary gland morphogenesis and tumorigenesis: insights from imaging. Histochem Cell Biol. 2008;130:1105–18.

[42] Zhang Y, Gordon A, Qian W, Chen W. Engineering nanoscale stem cell niche: direct stem cell behavior at cell-matrix interface. Adv Healthc Mater. 2015;4(13):1900–14.

[43] Morgan BA. The dermal papilla: an instructive niche for epithelial stem and progenitor cells in development and regeneration of the hair follicle. Csh Perspect Med. 2014; 4: a15180.

[44] Thornton C, Leaw B, Mallard C, Nair S, Jinnai M, Hagberg H. Cell Death in the Developing Brain after Hypoxia-Ischemia. Front Cell Neurosci. 2017;11:248.

[45] Williams ML, Bhatia SK. Engineering the extracellular matrix for clinical applications: endoderm, mesoderm, and ectoderm. Biotechnol J. 2014;9(3):337–47.

[46] Bronzino JD, Schaffer DV, Peterson DR. Stem cell engineering: principles and practices. Boca Raton: CRC Press; 2013.

[47] Wang H, Hansen MB, Löwik DWPM, van Hest JCM, Li Y, Jansen JA, et al. Oppositely charged gelatin nanospheres as building blocks for injectable and biodegradable gels. Adv Mater. 2011;23(12):H119–24.

[48] Sharma C, Dinda AK, Potdar PD, Chou C-F, Mishra NC. Fabrication and characterization of novel nano-biocomposite scaffold of chitosan-gelatin-alginate-hydroxyapatite for bone tissue engineering. Mater Sci Eng C Mater Biol Appl. 2016;64:416–27.

[49] Kageyama T, Yoshimura C, Myasnikova D, Kataoka K, Nittami T, Maruo S, et al. Spontaneous hair follicle germ (HFG) formation in vitro, enabling the large-scale production of HFGs for regenerative medicine. Biomaterials 2018;154:291–300.

[50] Balana ME, Charreau HE, Leiros GJ. Epidermal stem cells and skin tissue engineering in hair follicle regeneration. World J Stem Cells. 2015;7:711–27.

[51] Chen P, Zhang F, Fan Z, Shen T, Liu B, Chen R, et al. Nanoscale microenvironment engineering for expanding human hair follicle stem cell and revealing their plasticity. J Nanobiotechnol. 2021;19(1). doi: https://doi.org/10.1186/s12951-021-00840-5.